

Article

Optimal Configuration of Multi-Energy Storage in an Electric–Thermal–Hydrogen Integrated Energy System Considering Extreme Disaster Scenarios

Zhe Chen ¹, Zihan Sun ², Da Lin ¹ , Zhihao Li ¹ and Jian Chen ^{2,*} 

¹ State Grid Zhejiang Electric Power Research Institute, Hangzhou 310014, China; zchen331@163.com (Z.C.); ld2009ee@163.com (D.L.); lizhh17@zju.edu.cn (Z.L.)

² Key Laboratory of Power System Intelligent Dispatch and Control of Ministry of Education, Shandong University, Jinan 250061, China; szh20016@163.com

* Correspondence: ejchen@sdu.edu.cn

Abstract: Extreme disasters have become increasingly common in recent years and pose significant dangers to the integrated energy system's secure and dependable energy supply. As a vital part of an integrated energy system, the energy storage system can help with emergency rescue and recovery during major disasters. In addition, it can improve energy utilization rates and regulate fluctuations in renewable energy under normal conditions. In this study, the sizing scheme of multi-energy storage equipment in the electric–thermal–hydrogen integrated energy system is optimized; economic optimization in the regular operating scenario and resilience enhancement in extreme disaster scenarios are also considered. A refined model of multi-energy storage is constructed, and a two-layer capacity configuration optimization model is proposed. This model is further enhanced by the integration of a Markov two-state fault transmission model, which simulates equipment defects and improves system resilience. The optimization process is solved using the tabu chaotic quantum particle swarm optimization (TCQPSO) algorithm to provide reliable and accurate optimization results. The results indicate that addressing severe disaster situations in a capacity configuration fully leverages the reserve energy function of energy storage and enhances system resilience while maintaining economic efficiency; furthermore, adjusting the load loss penalty coefficients offers a more targeted approach to the balancing of the system economy and resilience. Thus, new algorithmic choices and planning strategies for future research on enhancing the resilience of integrated energy systems under extreme disaster scenarios are provided.

Keywords: extreme disasters; resilience; two-layer optimal configuration model; tabu chaotic quantum particle swarm optimization



Citation: Chen, Z.; Sun, Z.; Lin, D.; Li, Z.; Chen, J. Optimal Configuration of Multi-Energy Storage in an Electric–Thermal–Hydrogen Integrated Energy System Considering Extreme Disaster Scenarios. *Sustainability* **2024**, *16*, 2276. <https://doi.org/10.3390/su16062276>

Academic Editor: Mohammed Elsayed Lotfy

Received: 5 February 2024

Revised: 1 March 2024

Accepted: 6 March 2024

Published: 8 March 2024



Copyright: © 2024 by the authors. Licensee MDPI, Basel, Switzerland. This article is an open access article distributed under the terms and conditions of the Creative Commons Attribution (CC BY) license (<https://creativecommons.org/licenses/by/4.0/>).

1. Introduction

In the context of the energy internet and dual carbon objectives, integrated energy systems (IES) have gained significant attention and have undergone rapid development [1–3]. The integrated energy system makes extensive use of renewable energy, enhances energy efficiency, and lowers carbon emissions through multi-energy coupling. Among these systems, the electric–thermal–hydrogen integrated energy system, as an efficient, clean, and sustainable energy usage technique, has recently become the focus of study in the field of integrated energy. Energy storage systems serve as a vital link between the supply and demand of integrated electric, thermal, and hydrogen energy. They can effectively stabilize the uncertainty of renewable energy, facilitate load peak–valley transfer, and minimize the need for a backup power supply installation. It is a useful strategy for raising the percentage of renewable energy used [4,5]. At the same time, energy storage devices can be used to store and release energy in the event of a major disaster, ensuring a steady supply of energy.

The energy storage configuration problem is closely coupled with the operation problem. Scholars have carried out extensive research on energy storage operations [6–8]. Compared with the traditional energy storage battery, the integrated energy system introduces a multi-energy storage system, including power storage, heat storage, hydrogen storage, and composite energy storage. In [9], a multi-energy microgrid scheduling approach, including electricity, heat, and gas multi-energy storage, was constructed; the approach took renewable energy and load unpredictability into account. In [10], the authors provided an autonomous optimal microgrid operation strategy based on the previously established electric–thermal–hydrogen energy storage model; the study considers the interacting power limit between the microgrid, the external power grid, and the heating network. In [11], which considers the influence of electric energy storage and the system operation costs, an economic operation model of a microgrid, which included wind power generation equipment, photovoltaic power generation equipment, waste heat boilers, and batteries, was established to ensure the economic operation of the system. Considering the seasonal differences in load and renewable energy output, Ref. [12] established a regional IES, which included a seasonal thermal energy storage system; the scheduling was optimized, which solved the seasonal imbalance between heat load supply and demand and improved the overall efficiency of the system. The above studies mainly consider simplified models of the equipment; thus, it is necessary to develop a refined model based on the specific operating conditions of each piece of equipment. At the same time, most of the studies do not address the life degradation of electrothermal hydrogen equipment, and there are few investigations on related models of life degradation.

Based on the operational problems, the capacity of the energy storage system must be configured to further ensure the system’s stability, reliability, and economic operation. Through acceptable energy storage capacity configuration and operating strategies, the energy utilization efficiency can be further increased, the energy cost can be decreased, and significant support can be offered for low-carbon and sustainable development [13,14]. In [15], a study that considered the economy and environmental protection of the system, a bi-objective mixed integer nonlinear optimum allocation model was constructed that took into account the economic and environmental goals established by the life cycle analysis; the overall goal was defined as the weighted total of each individual goal. In [16], the authors established a deviation adaptation approach based on economics and carbon emissions; the approach was then applied to the planning and scheduling of gas, wind, solar, and hydrogen energy in integrated energy systems in order to increase the systems’ economy and environmental protection. In [17], an optimization configuration method using an integrated energy system was proposed to consider the additional potential benefits of energy storage. Based on the peak load shifting characteristics of energy storage, the additional potential benefits of the energy storage model were established by further considering the changes in the system load and real-time electricity price. The above studies mainly focused on improving system economy, with little regard for system reliability and security. Secondly, in terms of solution algorithms, intelligent algorithms such as the genetic algorithm and the particle swarm optimization algorithm are widely used. In [18], a partition optimization configuration method combining K-means and a genetic algorithm was proposed for a regional integrated energy system that was composed of complex loads in order to configure the capacity of the energy storage equipment in the integrated energy system. In [19], the authors proposed an integrated energy system operation optimization method based on energy efficiency analysis and an adaptive genetic algorithm; using the adaptive genetic algorithm, they solved the problem of operation optimization. In [20], the energy loss in the transmission process was properly evaluated in the integrated energy system and incorporated into the objective function of the coordinated operation model. The study considered the non-convex nonlinear term of energy loss, and the genetic algorithm with a penalty function was used to solve the model. Most of the aforementioned studies resolved the capacity allocation problem using simple intelligent

algorithms; however, by mixing several intelligent algorithms, the accuracy and speed of the solution can be further increased.

In summary, in the existing optimal configuration of integrated energy multi-energy storage, most of the studies have not constructed a refined model of the equipment that takes life degradation into account, and the configuration goal is mainly based on economy, ignoring the improvement of system resilience. At the same time, the method applied to solving the mixed integer linearization problem of double-layer capacity optimization configuration is limited. Therefore, in order to rationalize the configuration capacity of multi-energy storage by considering the occurrence of extreme disasters in the planning configuration, with the aim of improving the resilience of the integrated energy system and effectively reducing the loss of various types of loads when extreme disasters occur, this study makes further improvements in terms of the refinement of equipment models, the comprehensiveness of the capacity configuration considerations, and the accuracy of the model solving methods.

The main contributions of this study are summarized as follows:

(1) This study presents a revised model of an electrolytic cell and a fuel cell and considers climbing, power, temperature, start–stop, and other parameters. Simultaneously, the life degradation model is developed to consider the aging mechanisms of the battery, electrolytic cell, and fuel cell and to imitate the operational state and operating characteristics of multi-element energy storage equipment more correctly.

(2) This study constructs a two-layer optimal configuration model of a multi-energy storage system. The upper layer is the capacity configuration, and the equipment capacity configuration scheme is given to guide the optimal operation of each piece of equipment in the lower layer. At the same time, in the configuration layer, extreme disaster scenarios such as hurricanes are added based on a consideration of the existing normal scenarios; thus, the configuration results can improve the resilience of the system to a certain extent while ensuring the economy of the system.

(3) This study resolves the two-layer capacity configuration model using the tabu chaotic particle swarm optimization algorithm. The chaos algorithm, tabu algorithm, and particle swarm optimization method are integrated. When compared to the conventional particle swarm optimization method, the three algorithms' advantages are fully integrated to enhance the algorithm's capacity for both local and global search, as well as to guarantee the accuracy of the result.

2. Refined Model of Multivariate Energy Storage

The integrated energy system integrates various energy sources (Figure 1). It relies heavily on a multifaceted energy storage apparatus to connect integrated energy input with demand. The development of the system's model significantly influences the subsequent optimization of the system's operations. In the electric–thermal–hydrogen integrated energy system, refined models of the electric energy storage, thermal energy storage, hydrogen energy storage, multi-type electrolyzer, and multi-type hydrogen fuel cell are established, and the life degradation characteristics of the electric energy storage, electrolyzer, and hydrogen fuel cell are considered and modeled.

2.1. Electricity Storage

2.1.1. Life Degradation Model

The life of the battery is closely related to the state of charge as well as the charging and discharging power. The life of the battery can be formulated as the sum of the effective throughput available to the battery. When the accumulated effective throughput reaches the rated life of the battery, the battery needs to be replaced. The rated available throughput of the battery is as follows:

$$\Gamma_R = L_R D_R C_R \quad (1)$$

where Γ_R represents the rated throughput of the battery, L_R represents the rated cycle life, D_R represents the rated discharge depth, and C_R represents the rated capacity under the rated discharge current.

$$\begin{cases} d_{\text{eff}} = k_0(1 - k_1 S_t + k_2 S_t^2) \\ k_0 = \exp(u_1 - 1 + 1/D_R) d_R / D_R^{u_0} \\ k_1 = u_0 + u_1 / D_R \\ k_2 = u_0(u_0 - 1) / 2 + u_0 u_1 / D_R + u_1^2 / 2 D_R^2 \end{cases} \quad (2)$$

Here, d_{eff} represents the throughput consumed by using a battery; d_R is the rated throughput consumed by a single discharge; u_0 and u_1 are the parameters obtained in the simulation process; and k_0 , k_1 , and k_2 are constants obtained from the battery parameters.

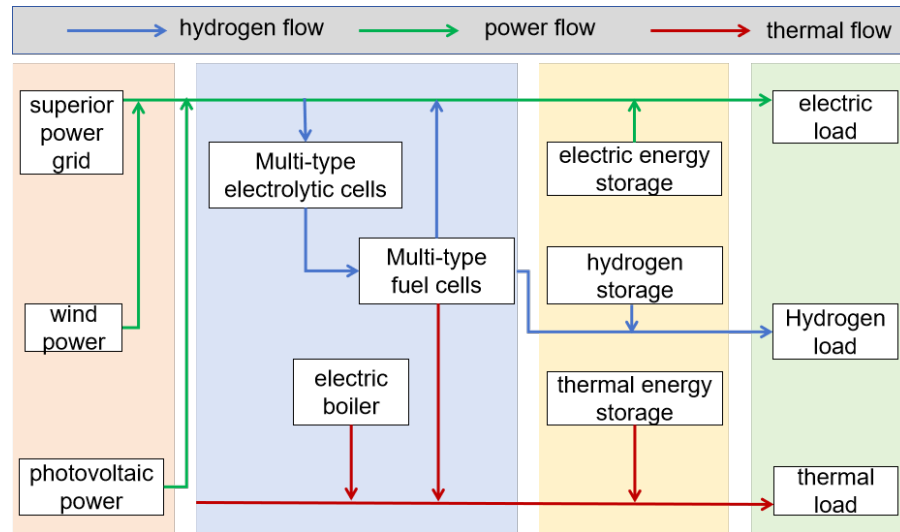


Figure 1. Basic equipment of an electrothermal hydrogen integrated energy system.

2.1.2. Basic Model

When establishing the basic model of the battery, the life degradation must be considered; it is also necessary to satisfy the basic constraints of the energy storage equipment, such as the charging and discharging power constraints, efficiency constraints, and battery capacity constraints. The specific formula is as follows:

$$\begin{cases} E_{\min} \leq E_t \leq E_{\max} \\ E_t = E_{t-1} - P_{\text{dis},t} \Delta t / \eta_{\text{dis}} + \eta_{\text{ch}} P_{\text{ch},t} \\ E_T = E_0 \\ 0 \leq P_{\text{ch},t} \leq P_{\text{ch}}^{\max} B_{\text{ch},t} \\ 0 \leq P_{\text{dis},t} \leq P_{\text{dis}}^{\max} B_{\text{dis},t} \\ B_{\text{ch},t} + B_{\text{dis},t} \leq 1 \end{cases} \quad (3)$$

where E_t represents the battery power at the moment at time t ; $P_{\text{dis},t}$ and $P_{\text{ch},t}$ represent the charging and discharging heat power of the battery at time t ; η_{dis} and η_{ch} represent the charging and discharging efficiency of the battery; $P_{\text{max}}^{\text{ch}}$ and $P_{\text{max}}^{\text{dis}}$ represent the maximum power limit of the charging and discharging of the battery; E_{\max} and E_{\min} represent the upper and lower limits of the capacity of the heat storage tank; and $B_{\text{ch},t}$ and $B_{\text{dis},t}$ represent the charging and discharging sign.

2.2. Thermal/Hydrogen Storage

As with the basic operation model of electric energy storage, thermal energy storage and hydrogen energy storage need to meet the following constraints during operation:

$$\begin{cases} H_{\min} \leq H_t \leq H_{\max} \\ H_t = H_{t-\Delta t} - Q_t^{\text{dis}} \Delta t / \eta_{\text{heat}}^{\text{dis}} + \eta_{\text{heat}}^{\text{ch}} Q_t^{\text{ch}} \Delta t \\ H_T = H_0 \\ 0 \leq Q_t^{\text{ch}} \leq Q_{\max}^{\text{ch}} A_t^{\text{ch}} \\ 0 \leq Q_t^{\text{dis}} \leq Q_{\max}^{\text{dis}} A_t^{\text{dis}} \\ A_t^{\text{ch}} + A_t^{\text{dis}} \leq 1 \end{cases} \quad (4)$$

$$\begin{cases} m_{\min}^{\text{HST}} \leq m_t^{\text{HST}} \leq m_{\max}^{\text{HST}} \\ m_{t+1}^{\text{HST}} = m_t^{\text{HST}} - m_t^{\text{HST},\text{out}} / \eta_{\text{out}}^{\text{HST}} + \eta_{\text{in}}^{\text{HST}} Q_t^{\text{HST},\text{in}} \\ m_T^{\text{HST}} = m_0^{\text{HST}} \\ 0 \leq m_t^{\text{HST},\text{in}} \leq m_{\max}^{\text{HST},\text{in}} B_t^{\text{HST},\text{in}} \\ 0 \leq m_t^{\text{HST},\text{out}} \leq m_{\max}^{\text{HST},\text{out}} B_t^{\text{HST},\text{out}} \\ 0 \leq B_t^{\text{HST},\text{out}} + B_t^{\text{HST},\text{in}} \leq 1 \end{cases} \quad (5)$$

2.3. Electro-Hydrogen Coupling Equipment

2.3.1. Life Degradation Model

The continuous operation of the electro-hydrogen coupling equipment leads to the life degradation of the electro-hydrogen coupling equipment. At present, it is difficult to directly establish an accurate mathematical model for the life degradation of the electro-hydrogen coupling equipment. Life degradation is indirectly reflected by measuring the voltage change through experimentation. This is because when the electro-hydrogen coupling equipment is running, the catalytic layer undergoes irreversible loss, the membrane resistance becomes larger, and the overpotential of the electro-hydrogen coupling equipment increases. Under the condition that the output hydrogen flow rate is constant, it is necessary to keep the current constant, and the increase in the operating voltage means that the working efficiency of the electro-hydrogen coupling equipment decreases. When the working voltage of the electro-hydrogen coupling device rises to the maximum working voltage, the electro-hydrogen coupling device needs to be replaced in order to ensure system efficiency [21]. Research shows that the voltage changes in the electro-hydrogen coupling device are closely related to its power fluctuations when parameters such as temperature and pressure are determined.

$$\begin{cases} D_{1,t}^{\text{EC}} = \lambda_1^{\text{EC}} U_t^{\text{EC}} \\ D_{2,t}^{\text{EC}} = \lambda_2^{\text{EC}} |P_t^{\text{EC}} - P_{t-1}^{\text{EC}}| / P_{\text{rate}}^{\text{EC}} \\ D_{3,t}^{\text{EC}} = \lambda_3^{\text{EC}} (A_{\text{on},t}^{\text{EC}} + A_{\text{off},t}^{\text{EC}}) \\ D^{\text{EC}} = \sum_{t=1}^T (D_{1,t}^{\text{EC}} \Delta t + D_{2,t}^{\text{EC}} / \Delta t + D_{3,t}^{\text{EC}}) \\ L_{\text{de}}^{\text{EC}} = D^{\text{EC}} / \lambda_{\text{rate}}^{\text{EC}} \\ L_{\text{rate}}^{\text{EC}} = \eta_{\text{rate}}^{\text{EC}} - \eta_{\text{lim}}^{\text{EC}} / \lambda_{\text{rate}}^{\text{EC}} \end{cases} \quad (6)$$

Here, $\lambda_1^{\text{EC/FC}}$, $\lambda_2^{\text{EC/FC}}$, and $\lambda_3^{\text{EC/FC}}$ are the efficiency degradation coefficients of the electro-hydrogen coupling equipment during steady operation, fluctuating operation, and start-stop, respectively. In this study, they are set to 2.75×10^{-7} , 2.75×10^{-6} , and 5.50×10^{-6} , respectively. $D_{1,t}^{\text{EC/FC}}$, $D_{2,t}^{\text{EC/FC}}$, and $D_{3,t}^{\text{EC/FC}}$ are the efficiency degradation of the electro-hydrogen coupling equipment during steady operation, fluctuating operation, and start-stop, respectively. $D^{\text{EC/FC}}$ and $L_{\text{de}}^{\text{EC/FC}}$ represent the total efficiency degradation and equivalent life degradation of the electro-hydrogen coupling equipment when running a scheduling cycle.

2.3.2. Start–Stop Model

$$\begin{cases} A_{\text{on},t-\alpha}^{\text{FC/EC}} - A_{\text{off},t}^{\text{FC/EC}} = U_t^{\text{FC/EC}} - U_{t-\Delta t}^{\text{FC/EC}} \\ A_{\text{on},t}^{\text{FC/EC}} \leq 1 - U_{t-\Delta t}^{\text{FC/EC}} \\ A_{\text{off},t}^{\text{FC/EC}} \leq U_{t-\Delta t}^{\text{FC/EC}} \end{cases} \quad (7)$$

$$\begin{cases} \sum_{t=1}^T A_{\text{on},t}^{\text{FC/EC}} \leq A_{\text{on},\text{max}}^{\text{FC/EC}} \\ \sum_{t=1}^T A_{\text{off},t}^{\text{FC/EC}} \leq A_{\text{off},\text{max}}^{\text{FC/EC}} \end{cases} \quad (8)$$

The 0–1 variable $U_t^{\text{EC/FC}}$ represents the on–off state of the electro-hydrogen coupling equipment; $A_{\text{on},t}^{\text{EC/FC}}$ and $A_{\text{off},t}^{\text{EC/FC}}$ represent the start-up action and start–stop action of the electro-hydrogen coupling equipment, respectively; $\alpha^{\text{EC/FC}}$ denotes the start-up delay of the electro-hydrogen coupling equipment; and $A_{\text{on},\text{max}}^{\text{EC/FC}}$ and $A_{\text{off},\text{max}}^{\text{EC/FC}}$ represent the upper limit of the number of start-ups and shutdowns of the electro-hydrogen coupling equipment within a day, respectively.

2.3.3. Heat Transfer Model

$$T_{t+\Delta t}^{\text{EC/FC}} = T_t^{\text{EC/FC}} + (Q_t^{\text{EC/FC}} - Q_{\text{loss},t}^{\text{EC/FC}} - Q_{\text{move},t}^{\text{EC/FC}}) \Delta t / C^{\text{EC/FC}} \quad (9)$$

$$Q_{\text{loss},k,t}^{\text{EC/FC}} = (T_{k,t}^{\text{EC/FC}} - T_{k,a}^{\text{EC/FC}}) / R^{\text{EC/FC}} \quad (10)$$

$$T_{\text{min}}^{\text{EC/FC}} \leq T_{k,t}^{\text{EC/FC}} \leq T_{\text{max}}^{\text{EC/FC}} \quad (11)$$

Here, $T_a^{\text{EC/FC}}$ represents the external temperature of the electro-hydrogen coupling equipment; $C^{\text{EC/FC}}$ represents the lumped heat capacity; $R^{\text{EC/FC}}$ represents the thermal resistance; $Q_{\text{loss},t}^{\text{EC/FC}}$ represents the thermal power lost by the electro-hydrogen coupling equipment; $Q_{\text{move},t}^{\text{EC/FC}}$ represents the thermal power outside the output system; $T_t^{\text{EC/FC}}$ is the temperature; and $T_{\text{max}}^{\text{EC/FC}}$ and $T_{\text{min}}^{\text{EC/FC}}$ are the upper and lower limits of the temperature of the electro-hydrogen coupling equipment, respectively.

2.3.4. Output Model

$$P_{k,t}^{\text{EC/FC}} \geq (U_{k,t}^{\text{EC/FC}} P_{\text{min}}^{\text{EC/FC}} + \sum_{\tau=0}^{\alpha^{\text{EC/FC}} - \Delta t} A_{\text{on},k,t-\tau}^{\text{EC/FC}} P_{\text{boot}}^{\text{EC/FC}}) \quad (12)$$

$$P_{k,t}^{\text{EC/FC}} \leq (U_{k,t}^{\text{EC/FC}} P_{\text{max}}^{\text{EC/FC}} + \sum_{\tau=0}^{\alpha^{\text{EC/FC}} - 1} A_{\text{on},k,t-\tau}^{\text{EC/FC}} P_{\text{boot}}^{\text{EC/FC}}) \quad (13)$$

$$\left| P_{k,t}^{\text{EC/FC}} - P_{k,t-1}^{\text{EC/FC}} \right| \leq U_{k,t}^{\text{EC/FC}} \Delta P_{\text{max}}^{\text{EC/FC}} + (1 - U_{k,t}^{\text{EC/FC}}) P_{\text{max}}^{\text{EC/FC}} \quad (14)$$

Here, $P_{\text{max}}^{\text{EC/FC}} / P_{\text{min}}^{\text{EC/FC}}$ represent the upper/lower limit of the operating power of the electro-hydrogen coupling equipment in the on state; $P_{\text{boot}}^{\text{EC/FC}}$ represents the power consumed during the start-up of the electro-hydrogen coupling equipment; $\Delta P_{\text{max}}^{\text{EC/FC}}$ represents the maximum climbing power per unit period of the electro-hydrogen coupling equipment in the boot state; and $P_{\text{max}}^{\text{EC/FC}}$ represents the upper limit of its working power.

2.3.5. Power Model

The working efficiency models of the electrolytic cell and hydrogen fuel cell are shown as follows:

$$\begin{cases} m_{k,t}^{\text{M,H}_2} = \eta_{\text{ele},k,t}^{\text{M}} P_{k,t}^{\text{M}} U_{k,t}^{\text{M}} \Delta t / \gamma \\ Q_{k,t}^{\text{M}} = \eta_{\text{heat},k,t}^{\text{M}} P_{k,t}^{\text{M}} \end{cases} \quad (15)$$

$$\begin{cases} P_t^{FC} = (\gamma m_{H2,t}^{FC}) / \Delta t \\ P_{ele,t}^{FC} = \eta_{ele}^{FC} P_t^{FC} U_t^{FC} \\ Q^{FC} = \eta_{heat}^{FC} P_t^{FC} \end{cases} \quad (16)$$

2.4. Sequential Monte Carlo Extraction Equipment Fault Model Based on Markov State Transition

2.4.1. Markov State Transformation Model

Outdoor wind turbines and photovoltaic equipment are more susceptible to damage during extreme catastrophes like hurricanes compared to indoor integrated energy equipment. This vulnerability ultimately leads to forced outages. Considering that most of the forced outages of equipment caused by extreme disasters such as hurricanes are repairable, this study uses the Markov two-state transition model to describe the probability characteristics of wind turbines and photovoltaic equipment, which can be simulated by the steady-state ‘operation-failure-operation’ cycle process (Figure 2). Firstly, the failure rate of the equipment is introduced. At the same time, it takes a certain amount of time to repair the faulty equipment after the failure occurs (Figure 3). Therefore, the repair rate of the equipment is introduced. The established equipment failure model based on the Markov two-state transition is as follows:

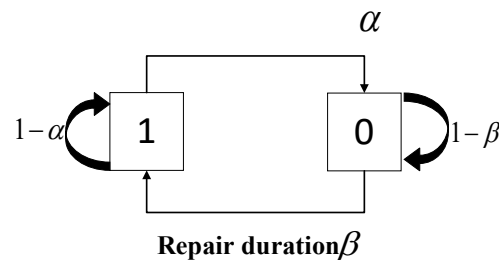


Figure 2. Markov two-state transition equipment fault model.

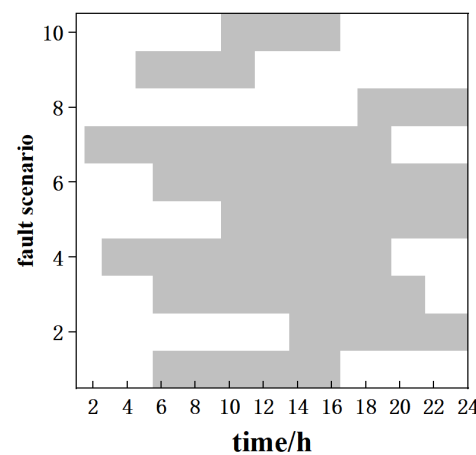


Figure 3. Equipment fault extraction results based on sequential Monte Carlo.

2.4.2. Equipment Fault Extraction Model Based on Sequential Monte Carlo

Using the sequential Monte Carlo fault extraction model [22,23], the average outage time M_{TTF} is extracted according to the equipment failure rate λ , and the average repair time M_{TTR} is extracted according to the repair rate μ after the fault occurs. Then, the relationship can be interpreted as follows:

$$\lambda = 1/M_{TTF} \quad (17)$$

$$\mu = 1/M_{TTR} \quad (18)$$

Assuming that the duration of each state of the component obeys an exponential distribution, the probability density functions of the outage duration a and the repair duration b can be expressed as follows:

$$f(a) = \mu e^{-\mu a} \tag{19}$$

$$f(b) = \mu e^{-\mu b} \tag{20}$$

At the same time, the duration a and the repair duration b can be obtained by inverse transformation [24], as follows:

$$a = \frac{1}{\lambda} \ln \zeta_1 \tag{21}$$

$$b = \frac{1}{\mu} \ln \zeta_2 \tag{22}$$

In the formulae, ζ_1 and ζ_2 are random numbers with uniform distribution in the interval $[0, 1]$.

3. Two-Layer Capacity Optimization Configuration Model

The system bi-level optimal configuration model constructed in this study to consider economy and resilience is interconnected, as shown in Figure 4. Firstly, the upper capacity configuration layer transfers the initial capacity scheme of each device in the system to the lower optimal operation layer. The lower optimal operation layer adjusts the system scheduling according to the equipment capacity provided by the upper layer and feeds back the optimal value of the total operating cost to the upper layer as the basis for the upper layer to configure the new capacity scheme of each device. The upper and lower iterative cycles finally obtain the optimal configuration scheme and the optimal operation results.

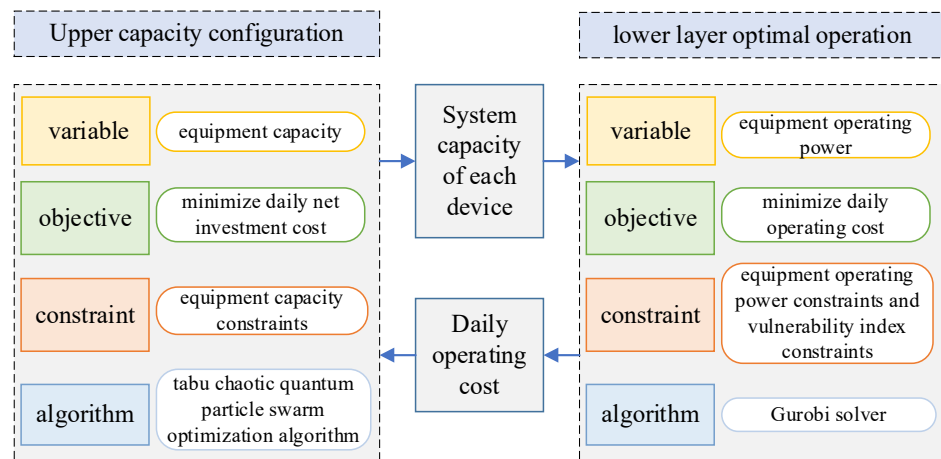


Figure 4. Two-layer capacity optimization configuration model.

3.1. Capacity Configuration Model

The objective function of the upper-level capacity allocation is to maximize daily net income, where the daily net income is equal to the daily operating income obtained by the lower-level optimization operation minus the system investment cost. By designing the capacity of the various equipment parts (battery, heat storage tank, hydrogen storage tank, fuel cell, and multi-type electrolytic cell) of the electrothermal hydrogen integrated energy system, the daily net profit of the system is maximized. The specific objective function expression is as follows:

$$\min F_{con} = \min(C_{in}/365 - F) \tag{23}$$

$$C_{in} = \sum_{i=1}^N \left[\zeta_i S_i \eta_i (1 + \eta_i)^{t_i} / \left((1 + \eta_i)^{t_i} - 1 \right) \right] \tag{24}$$

where F_{con} represents the objective function of the upper optimization design; F represents the objective function of the lower-level optimal operation; C_{in} represents the system investment cost; N represents the total number of equipment parts in the integrated energy system; η_i represents the interest rate, taken as 5%; ξ_i represents the investment cost per unit capacity of each equipment part; and S_i represents the capacity of each equipment part in the integrated energy system.

3.2. Capacity Configuration Constraints

Regarding the constraints of the construction scale and construction conditions, the constraints of the upper capacity configuration model include capacity constraints such as energy conversion equipment (multi-type electrolyzers and hydrogen fuel cells) and energy storage equipment (hydrogen storage tanks, heat storage tanks, and batteries). The expression is as follows:

$$S_i^{\min} \leq S_i \leq S_i^{\max} \quad (25)$$

3.3. Optimal Operating Model

The optimization goal of this study is to improve the economy and toughness of the electrothermal hydrogen system in each scenario and to consider the life improvement of the electrolytic cell and the battery. The objective function includes the operating cost and the equipment life loss cost.

$$\min F = F_{\text{life}} + F_{\text{op}} \quad (26)$$

$$F_{\text{life}} = \sum_{\kappa}^K \left[\pi_{\kappa} (C_{\text{life}}^{\text{EC},\kappa} + C_{\text{life}}^{\text{FC},\kappa} + C_{\text{life}}^{\text{EES},\kappa}) \right] \quad (27)$$

Here, F_{life} represents the life loss cost; $C_{\text{life}}^{\text{EC},\kappa}$ represents the life loss cost of the electrolytic cell; $C_{\text{life}}^{\text{FC},\kappa}$ represents the life loss cost of the hydrogen fuel cell; and $C_{\text{life}}^{\text{EES},\kappa}$ represents the sum of the battery life loss cost and maintenance cost.

$$F_{\text{op}} = \sum_{\kappa}^K \left[\pi_{\kappa} (C_{\text{cur}}^{\kappa} + C_{\text{loss}}^{\kappa} + C_{\text{buy}}^{\kappa} + C_{\text{car}}^{\kappa} + C_{\text{sell}}^{\kappa}) \right] \quad (28)$$

Here, F_{op} represents the operating cost; K represents the number of scenes; π_{κ} represents the probability of scene κ ; and C_{cur}^{κ} , C_{loss}^{κ} , C_{buy}^{κ} , C_{car}^{κ} , and C_{sell}^{κ} represent the penalty cost of wind and light curtailment, the penalty cost of load shedding, the cost of electricity purchase, the penalty cost of carbon emission, and the profit from selling heat and hydrogen in the scenario, respectively. The system's resilience is mainly improved by controlling the minimum penalty cost of load shedding. The specific expressions are as follows:

$$\begin{cases} C_{\text{cur}}^{\kappa} = \sum_{t=1}^T c_{\text{re}}^{\text{cur}} (P_{\text{pv},\kappa,t}^{\text{cur}} + P_{\text{wt},\kappa,t}^{\text{cur}}) \\ C_{\text{loss}}^{\kappa} = \sum_{t=1}^T (c_{\text{ele}}^{\text{loss}} P_{\text{load},\kappa,t}^{\text{loss}} + c_{\text{heat}}^{\text{loss}} Q_{\text{load},\kappa,t}^{\text{loss}} + c_{\text{H2}}^{\text{loss}} m_{\text{H2},\kappa,t}^{\text{loss}}) \\ C_{\text{buy}}^{\kappa} = \sum_{t=1}^T (c_t^{\text{buy}} P_{\kappa,t}^{\text{buy}} - c_t^{\text{sell}} P_{\kappa,t}^{\text{sell}}) \\ C_{\text{car}}^{\kappa} = \sum_{t=1}^T (c^{\text{car}} \eta_{\text{ele-car}} P_{\kappa,t}^{\text{buy}}) \\ C_{\text{sell}}^{\kappa} = \sum_{t=1}^T (c_{\text{heat}}^{\text{sell}} Q_{\kappa,t}^{\text{sell}} + c_{\text{H2}}^{\text{sell}} m_{\text{H2},\kappa,t}^{\text{sell}}) \end{cases} \quad (29)$$

where c_t^{buy} and c_t^{sell} represent the unit prices of electricity purchase and sale, respectively; $P_{\kappa,t}^{\text{buy}}$ and $P_{\kappa,t}^{\text{sell}}$ represent the power of purchasing and selling electricity, respectively; $\eta_{\text{ele-car}}$ represents the conversion coefficient of electricity-carbon; C^{car} denotes the environmental penalty factor of carbon dioxide emissions; $c_{\text{re}}^{\text{cur}}$ denotes the penalty coefficient of wind and light abandonment; $P_{\text{pv},\kappa,t}^{\text{cur}}$ and $P_{\text{wt},\kappa,t}^{\text{cur}}$ represent the power of light curtailment and wind curtailment, respectively; $c_{\text{ele}}^{\text{loss}}$, $c_{\text{heat}}^{\text{loss}}$, and $c_{\text{H2}}^{\text{loss}}$ represent the penalty coefficients of the electrothermal hydrogen load, respectively; $P_{\text{load},\kappa,t}^{\text{loss}}$, $Q_{\text{load},\kappa,t}^{\text{loss}}$, and $m_{\text{load},\kappa,t}^{\text{H2,loss}}$ represent the load loss of electrothermal hydrogen, respectively; $c_{\text{heat}}^{\text{sell}}$ and $c_{\text{H2}}^{\text{sell}}$ represent the unit price of

selling heat and hydrogen, respectively; and $Q_{\kappa,t}^{\text{sell}}$ and $m_{\text{H2},\kappa,t}^{\text{sell}}$ represent the sold thermal power and hydrogen mass, respectively.

3.4. Operational Constraints

3.4.1. Wind Turbine Photovoltaic Output and Load Constraints

$$\begin{cases} P_{\kappa,t}^{\text{PV}} = \bar{P}_t^{\text{PV}} + \zeta_{\kappa,t}^{\text{PV}}, 0 \leq P_{\text{pv},\kappa,t}^{\text{cur}} \leq P_{\kappa,t}^{\text{PV}} \\ P_{\kappa,t}^{\text{wt}} = \bar{P}_t^{\text{wt}} + \zeta_{\kappa,t}^{\text{wt}}, 0 \leq P_{\text{wt},\kappa,t}^{\text{cur}} \leq P_{\kappa,t}^{\text{wt}} \\ P_{\kappa,t}^{\text{load}} = \bar{P}_t^{\text{load}} + \zeta_{\kappa,t}^{\text{ele}}, 0 \leq P_{\text{load},\kappa,t}^{\text{loss}} \leq P_{\kappa,t}^{\text{load}} \\ Q_{\kappa,t}^{\text{load}} = \bar{Q}_t^{\text{load}} + \zeta_{\kappa,t}^{\text{heat}}, 0 \leq Q_{\text{load},\kappa,t}^{\text{loss}} \leq Q_{\kappa,t}^{\text{load}} \\ m_{\text{H2},\kappa,t}^{\text{load}} = \bar{m}_{\text{H2},\kappa,t}^{\text{load}} + \zeta_{\kappa,t}^{\text{H2}}, 0 \leq m_{\text{load},\kappa,t}^{\text{H2,loss}} \leq m_{\text{H2},\kappa,t}^{\text{load}} \end{cases} \quad (30)$$

Here, $P_{\kappa,t}^{\text{PV}}$, $P_{\kappa,t}^{\text{wt}}$, $P_{\kappa,t}^{\text{load}}$, $Q_{\kappa,t}^{\text{load}}$, and $m_{\text{H2},\kappa,t}^{\text{load}}$ represent the actual values of the photovoltaic, wind turbine, and electrothermal hydrogen loads, respectively; \bar{P}_t^{PV} , \bar{P}_t^{wt} , \bar{P}_t^{load} , \bar{Q}_t^{load} , and $\bar{m}_{\text{H2},\kappa,t}^{\text{load}}$ represent the day-ahead predicted values of the photovoltaic, wind turbine, and electrothermal hydrogen load, respectively; and $\zeta_{\kappa,t}^{\text{PV}}$, $\zeta_{\kappa,t}^{\text{wt}}$, $\zeta_{\kappa,t}^{\text{ele}}$, $\zeta_{\kappa,t}^{\text{heat}}$ and $\zeta_{\kappa,t}^{\text{H2}}$ represent the prediction errors of the photovoltaic, wind turbine, and electrothermal hydrogen load, respectively.

3.4.2. Purchase and Sale Power Constraints

$$\begin{cases} 0 \leq P_{\kappa,t}^{\text{buy}} \leq P_{\text{max}}^{\text{buy}} U_{\kappa,t}^{\text{buy}} \\ 0 \leq P_{\kappa,t}^{\text{sell}} \leq P_{\text{max}}^{\text{sell}} U_{\kappa,t}^{\text{sell}} \\ U_{\kappa,t}^{\text{buy}} + U_{\kappa,t}^{\text{sell}} \leq 1 \end{cases} \quad (31)$$

Here, $U_{\kappa,t}^{\text{buy}}$ and $U_{\kappa,t}^{\text{sell}}$ respectively represent the state of the purchase and sale of electricity. $P_{\text{max}}^{\text{buy}}$ and $P_{\text{max}}^{\text{sell}}$ represent the upper limit of the purchase and sale power, respectively.

3.4.3. System Equilibrium Constraints

Electric power balance constraint:

$$\begin{cases} (P_{\kappa,t}^{\text{PV}} - P_{\text{pv},\kappa,t}^{\text{cur}}) + (P_{\kappa,t}^{\text{wt}} - P_{\text{wt},\kappa,t}^{\text{cur}}) - (P_{\kappa,t}^{\text{load}} - P_{\text{load},\kappa,t}^{\text{loss}}) \\ = P_{\kappa,t}^{\text{EC}} - P_{\text{ele},\kappa,t}^{\text{FC}} - P_{\kappa,t}^{\text{buy}} + P_{\kappa,t}^{\text{ch}} - P_{\kappa,t}^{\text{dis}} + P_{\kappa,t}^{\text{EB}} \end{cases} \quad (32)$$

Thermal power balance constraint:

$$\begin{cases} Q_{\kappa,t}^{\text{EC}} + Q_{\kappa,t}^{\text{FC}} + Q_{\kappa,t}^{\text{EB}} + Q_{\kappa,t}^{\text{dis}} - Q_{\kappa,t}^{\text{ch}} \\ = Q_{\kappa,t}^{\text{load}} - Q_{\text{load},\kappa,t}^{\text{loss}} + Q_{\kappa,t}^{\text{sell}} \end{cases} \quad (33)$$

Hydrogen mass balance constraint:

$$\begin{cases} m_{\text{H2},\kappa,t}^{\text{EC}} - m_{\text{H2},\kappa,t}^{\text{FC}} + m_{\text{H2},\text{out},\kappa,t}^{\text{HST}} - m_{\text{H2},\text{in},\kappa,t}^{\text{HST}} \\ = m_{\text{H2},\kappa,t}^{\text{load}} - m_{\text{H2},\kappa,t}^{\text{loss}} + m_{\text{H2},\kappa,t}^{\text{sell}} \end{cases} \quad (34)$$

4. Solution Method

The upper capacity configuration problem is solved using the tabu chaotic quantum particle swarm optimization approach. It has excellent computational accuracy, and with this approach, it is more difficult to fall into the local optimal solution than it is with the conventional particle swarm optimization approach. The approach involves complex and lengthy computation times, but these drawbacks can be mitigated with advanced techniques that balance its benefits. Firstly, the quantum method is mixed with the classical particle swarm optimization technique, and quantum bit superposition and entanglement

are used to speed up the search for the best solution. Secondly, to avoid finding the local optimal solution and to enhance both the local and global search capabilities, the taboo strategy in the taboo algorithm [25,26] and the quantum state representation and update process in the quantum particle swarm optimization algorithm [27,28] are combined.

The upper layer model transmits the configured capacity to the lower layer. The lower layer operation model calculates the output of each time period, uploads the obtained system operation cost to the upper layer capacity configuration model, and iterates it circularly. Finally, the capacity configuration scheme and optimal operation results that meet the economic and resilience requirements are outputs. The optimization process of the energy storage capacity configuration of the double-layer electrothermal hydrogen integrated energy system is shown in Figure 5.

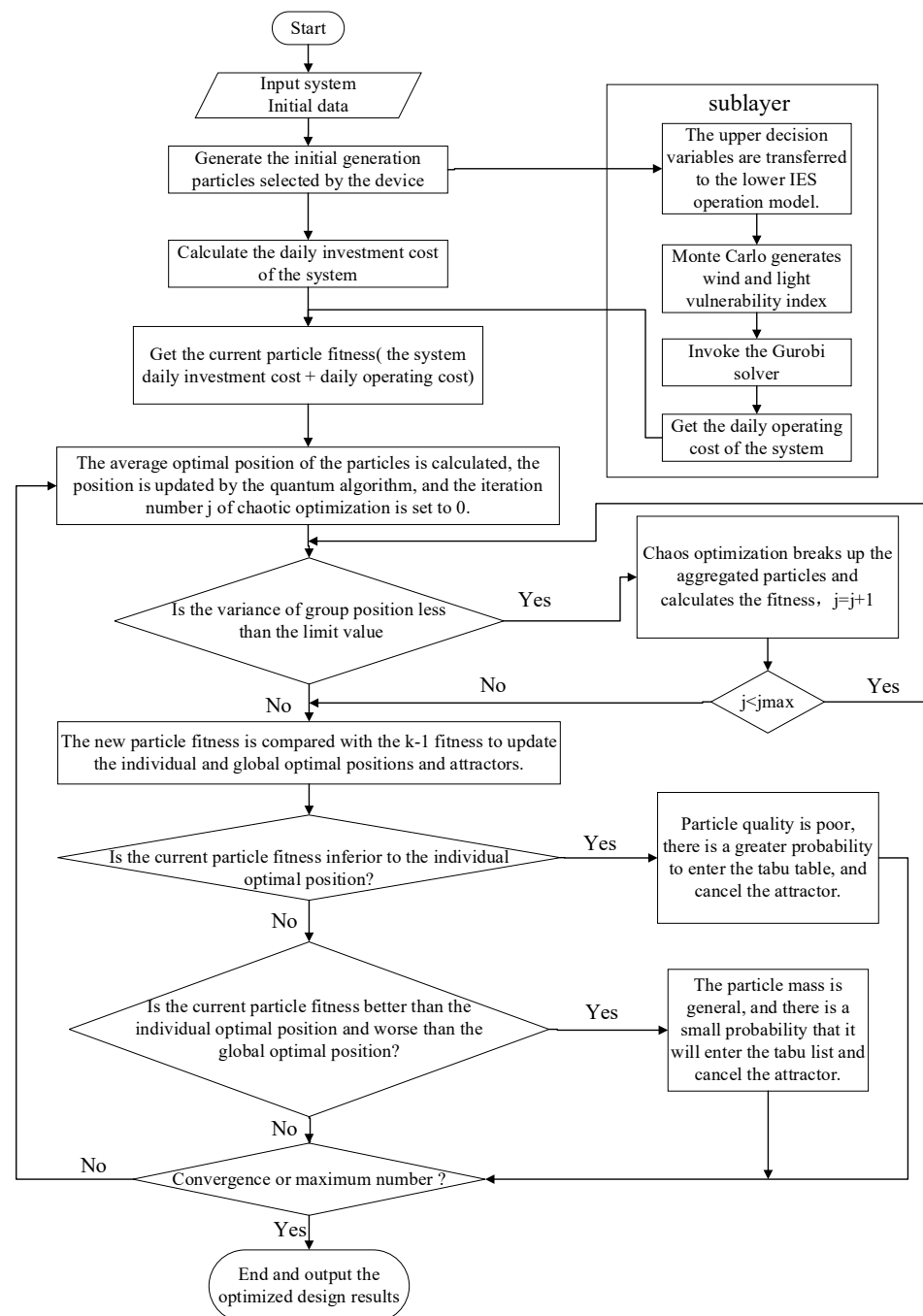


Figure 5. Two-layer capacity optimization configuration solution process.

The specific steps that need to be taken to solve the taboo chaotic quantum particle swarm are as follows:

STEP 1: Input the system's initial data.

STEP 2: The initial particles selected by the device, which correspond to each device's capacity, are generated and sent to the lower-level optimal operating model. Simultaneously, the lower-level optimum operation generates the wind and light vulnerability index using the Monte Carlo method and uses the Gurobi solver to solve it. The daily operating cost is obtained, and its value is returned to the upper layer.

STEP 3: The current particle fitness value, i.e., the system daily investment cost plus the daily operation cost, is obtained.

STEP 4: The average optimal position of the particles is calculated, the position is updated by the quantum algorithm, and the number of chaotic optimization iterations j is set to 0.

STEP 5: This step is to determine whether the variance of the group position is less than the limit value; if not, step 6 is entered. If yes, the chaotic optimization is used to break up the particles and recalculate the fitness, and $j = j + 1$, until the position variance is no longer less than the limit value or the maximum number of iterations of the chaotic optimization enters step 6.

STEP 6: The new particle fitness is compared with $k - 1$'s fitness, and the individual and global optimal positions and attractors are updated.

STEP 7: A judgement is made regarding whether the current particle fitness is inferior to the individual optimal position; if the current particle fitness is inferior to the individual optimal position, it is proved that the particle quality is poor, and there is a greater probability of entrance into the tabu table; then, the attractor is cancelled, and step 9 is entered. If the current fitness is better than the individual's optimal position, step 8 is entered.

STEP 8: This step is to determine whether the particle fitness is inferior to the global optimal position. If the current particle fitness value is inferior to the global optimal position, it is proved that the particle quality is general, and there is a small probability of entrance into the tabu table; then, the attractor is cancelled, and step 9 is entered. If it is superior to the global optimal position, it directly enters step 9.

STEP 9: This step is to determine whether to converge or to reach the maximum number of iterations. If so, the loop is ended, and the optimal design result is output. If not, step 4 is returned to, and the loop is started again.

5. Case Study

5.1. Overview of Examples

5.1.1. Parameters and Data

The electrothermal hydrogen/integrated energy system is constructed in this study. The parameters of the electrolyzer and fuel cell are shown in Table 1; the capacity configuration parameters of each device are shown in Table 2; and the parameters of the energy storage equipment are shown in Table 3.

Table 1. Operating parameters of EC and FC.

Equipment Variables	Electrolyzer	Hydrogen Fuel Cell
hydrogen/electricity production efficiency	0.65	0.45
heat production efficiency	0.3	0.5
lower limit of temperature/ $^{\circ}\text{C}$	50	25
upper limit of temperature/ $^{\circ}\text{C}$	80	100
upper/lower limit of output	1/0.05	1/0.05
upper climbing limit	100%/30 min	100%/30 min
maximum number of start-ups	2	2
maximum number of shutdowns	2	2
start-up delay	0 h	0 h

Table 2. Equipment capacity configuration parameters.

Equipment	Investment Cost	Upper Limit of Capacity	Lower Limit of Capacity	Term for Year
AEC	2400 (CNY/kW)	15 (MW)	5 (MW)	10
PEMEC	4000 (CNY/kW)	15 (MW)	5 (MW)	8
SOEC	6400 (CNY/kW)	15 (MW)	5 (MW)	5
PEMFC	4200 (CNY/kW)	5 (MW)	2 (MW)	5
SOFC	6300 (CNY/kW)	5 (MW)	2 (MW)	5
electric storage tank	1071 (CNY/kW)	20 (MW)	2 (MW)	10
heat storage tank	56 (CNY/kW)	30 (MW)	10 (MW)	25
hydrogen storage tank	65 (CNY/kg)	1000 (kg)	100 (kg)	35

Table 3. Energy storage equipment parameters.

Equipment	Charge/Discharge Efficiency	Energy Storage Range (%)	The Upper Limit of Charging/Discharging Rate (%)
electric storage tank	0.95/0.95	20–90	20
heat storage tank	0.95/0.95	10–90	20
hydrogen storage tank	0.95/0.95	30–80	10

5.1.2. Scene Setting

Based on the annual output data of the wind power generation equipment and the photovoltaic power generation equipment, we finally selected four typical days for analysis through the method of scene generation and reduction. When creating the capacity configuration of the extreme scenarios, the time period for the extreme scenarios was two days. The photovoltaic power generation and wind power generation equipment fault periods simulated by sequential Monte Carlo are shown in Table 4; the extreme weather and other harsh conditions in the actual situation are considered. There is a certain probability of occurrence; so, when considering the capacity configuration for the extreme scenarios, the fault probability is assigned to the total daily investment cost calculated by the two extreme scenarios to further ensure the accuracy of the configuration results. When the capacity configuration is not considered in extreme scenarios, all the devices work normally on four typical days.

Table 4. Equipment working and fault period in extreme scenarios.

Extreme Fault Scenarios	Normal Working Hours of PV	Fault Time of PV	Normal Working Hours of WT	Fault Time of WT
1	1–7 h, 19–24 h	8–18 h	1–7 h, 22–24 h	8–21 h
2	1–4 h, 24 h	5–23 h	1–4 h, 20–24 h	5–19 h

5.2. Analysis of Example Results

5.2.1. Upper Layer Capacity Configuration Results

Firstly, when only considering the normal scene, the particle swarm optimization algorithm and the tabu chaotic particle swarm optimization algorithm are used to solve the upper layer capacity configuration results, respectively. Fitness is the total cost of the daily investment, and when its value is negative, it shows that the day is in the system profit state. From the graph comparison, the total cost of the four typical days obtained by the particle swarm optimization algorithm is much higher than that obtained by the tabu chaotic quantum particle swarm optimization algorithm. As shown in Figure 6, the tabu chaotic quantum particle swarm optimization algorithm is superior to the basic particle swarm optimization algorithm in terms of both global and local search capabilities. Additionally, it is more difficult to fall into a local optimal solution, which ensures the accuracy of the solution results.

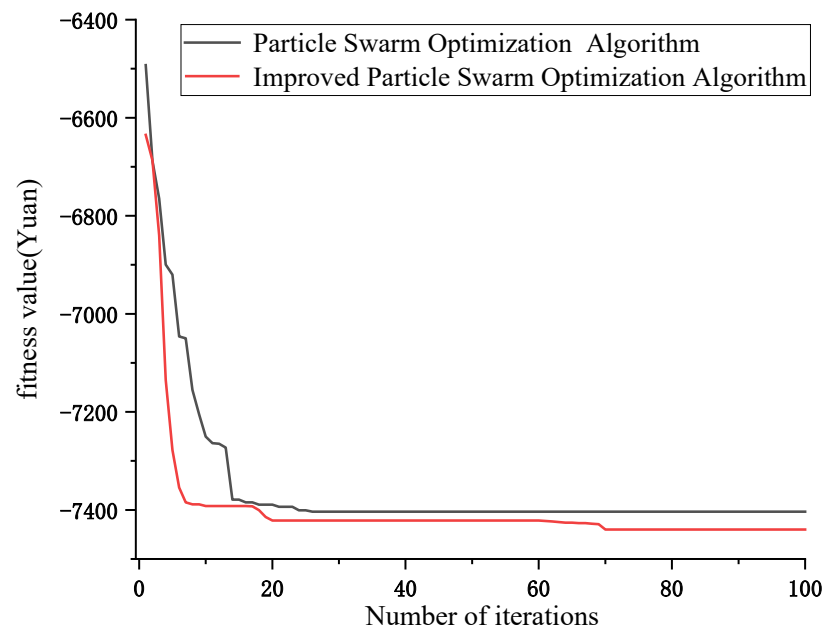


Figure 6. Comparison of upper–capacity solution algorithms.

Therefore, the tabu chaotic quantum particle swarm is used to solve the upper capacity configuration results for the different scenarios, as shown in Table 5. The basic settings of each example are as follows:

Case 1: Without considering the extreme disaster scenes, the four typical days are normal scenarios, which is a commonly used processing method in the existing research.

Case 2: Considering the extreme scenarios, the penalty coefficients of the electrical, thermal, and hydrogen load losses are all set to 1000.

Case 3: Considering the extreme scenarios, the penalty coefficients of the electrical, thermal, and hydrogen load losses are set at 1500-1000-1000.

Case 4: Considering the extreme scenarios, the penalty coefficients of the electrical, thermal, and hydrogen load losses are set to 1000-1500-1000.

Case 5: Considering the extreme scenarios, the penalty coefficients of the power, heat, and hydrogen losses are set at 1000-1000-1500.

Table 5. Upper capacity configuration results.

Case	AEC (MW)	PEMEC (MW)	SOEC (MW)	PEMFC (MW)	SOFC (MW)	HST (MW)	ESS (MW)	HSS (MW)
1	11	10	10	3	5	31	11	12
2	14	10	15	3	5	31	40	32
3	15	10	15	2	4	39	40	25
4	14	11	15	5	5	42	22	30
5	13	10	13	5	5	27	39	37

Through comparative analysis, after adding the extreme scenarios and comparing them with case 1, the configuration capacity of the energy storage equipment in the system increases to play the role of a standby power supply during the extreme disaster events. Secondly, by setting different load loss penalty coefficients, the configuration capacity of the energy storage can also be adjusted. In cases 3–5, by increasing the load loss penalty coefficients of the electricity, heat, and hydrogen in turn, the corresponding configuration capacities of the electric energy storage, thermal energy storage, and hydrogen energy storage also increase, which verifies the proposal that energy storage can play a role in reducing load loss when extreme events occur. At the same time, due to the coupling

between the subsystems of the electric–thermal–hydrogen integrated energy system studied here, the capacity of the electro-hydrogen coupling equipment is also affected when the extreme scenarios are considered and by the adjustment of the load loss penalty coefficient.

5.2.2. Optimal Operation Results of the Lower Layer

Load Loss Cost Analysis

Based on the premise that the configuration results of each equipment part in cases 1–5 are known, the load loss cost and operation cost of the lower optimal operation of cases 1–5 are further analyzed, as shown in Figures 7–10.

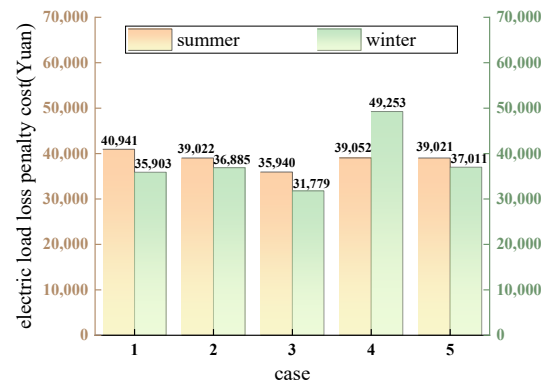


Figure 7. Electric load loss penalty cost.

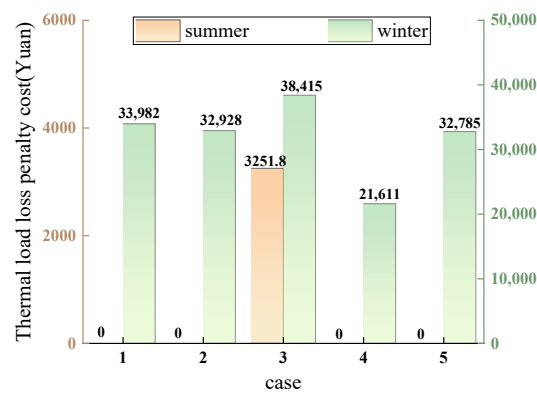


Figure 8. Thermal load loss penalty cost.

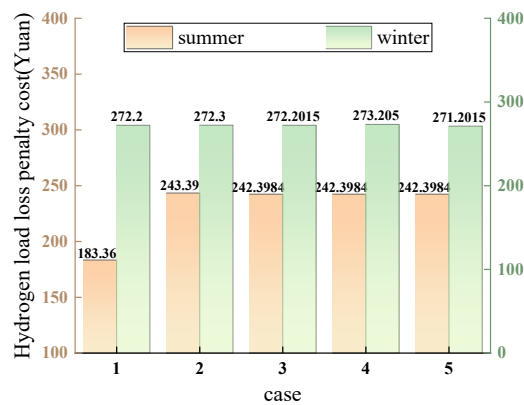


Figure 9. Hydrogen load loss penalty cost.

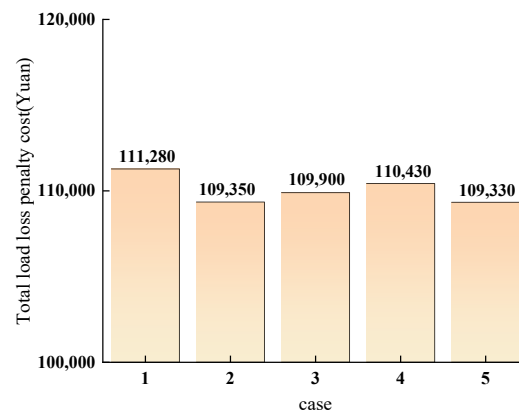


Figure 10. Total load loss penalty cost.

As shown in Figures 7–10, after considering the extreme disaster scenario in the upper capacity configuration, when facing extreme disaster events, the penalty cost of the power load loss and the heat load loss is greatly reduced, but the penalty cost of the hydrogen load loss is increased. When the emphasis is placed on reducing the various load losses, the penalty cost of the load loss can be further reduced by changing the penalty coefficient of the load loss; that is, the cost of the power load loss in example 3 is reduced; the cost of the heat load loss in example 4 is reduced; and the cost of the hydrogen load loss in example 5 is reduced. At the same time, because the fault time of the photovoltaic equipment and the wind turbine in fault scenario 2 is longer than that in fault scenario 1, it can be determined that the role of energy storage as a standby power supply is weakened, and the reduction range of the various load loss penalty costs is reduced; it is impossible to ensure that the load loss penalty costs of the various loads are reduced at the same time. However, compared with example 1, the penalty cost of the total loss of the various loads in the two days of examples 2–5 is still reduced.

Electric–Heat–Hydrogen Coupling Operation Analysis

Based on the premise that the upper layer capacity configuration is known, the optimal operation results of cases 1 and 2 in the normal scenarios and fault scenarios are further analyzed. Among them, fault scenario 1 is selected for further analysis. The fault periods of the photovoltaic equipment and wind turbines are 8–21 h and 8–18 h, respectively.

Through comparative analysis (Figures 11–14), in the fault scenario, whether to consider the extreme scenario configuration in the fault period of photovoltaic fan equipment reflects the difference. The output of the electric energy storage is greatly increased after configuration, while it is mainly in the charging state for the rest of the period, so that the system can meet the demand of the electric load to the greatest extent possible in order to reduce the loss of electric load. In addition to the role of electric energy storage in the fault period, the high-temperature solid oxide fuel cell can also provide a certain amount of electric energy. Secondly, compared with the unconfigured extreme scenario, the output of the electric boiler in the configured system is reduced, and the electric energy generated by the system is better stored in the battery. In the normal scenario, after considering the configuration of the fault scenario, the electric energy storage increases in each period, and the high-temperature solid oxide electrolytic cell consumes more electric energy. The output of the remaining equipment is similar to that of the unconfigured fault scenario.

The results of the thermal coupling operation are shown in Figures 15–18: when the extreme scenario configuration is disregarded, the heat storage tank and the high-temperature solid oxide fuel cell are primarily utilized to supply heat energy and satisfy the heat load demand during the fault period. After consideration of the extreme scenario configuration, it relies more on the high-temperature solid oxide electrolytic cell and the high-temperature solid oxide fuel cell to provide heat energy. One advantage is that both devices generate heat more efficiently while in operation. However, in contrast to the

heat storage tank, both devices are capable of fully converting alternative energy sources, thereby enhancing the overall efficiency of the energy conversion. In the normal scene, after considering the extreme scene configuration, the output of the proton exchange membrane electrolyzer decreases, the heat storage tank increases, and the output of the other equipment is similar.

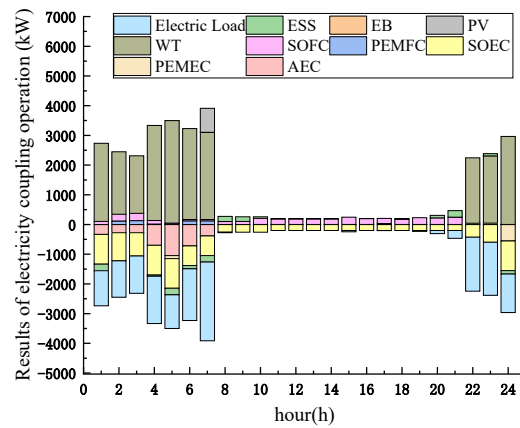


Figure 11. Electrical coupling operation results from fault scenarios without considering the configuration of extreme scenarios.

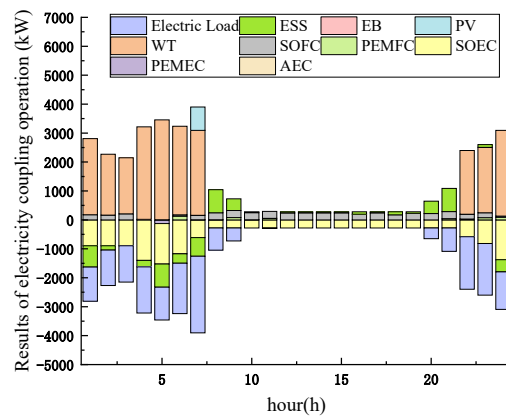


Figure 12. Electrical coupling operation results from fault scenarios considering the configuration of extreme scenarios.

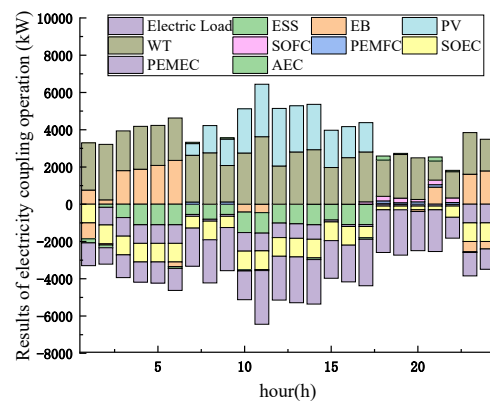


Figure 13. Electrical coupling operation results from normal scenarios without considering the configuration of extreme scenarios.

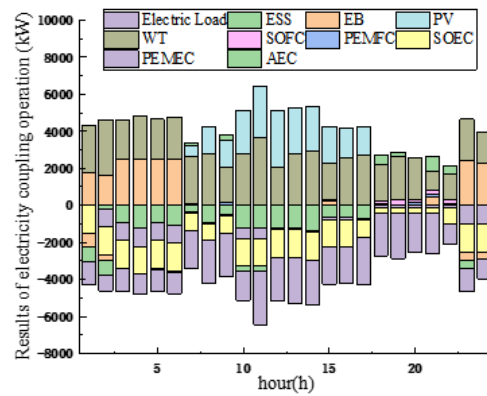


Figure 14. Electrical coupling operation results from normal scenarios considering the configuration of extreme scenarios.

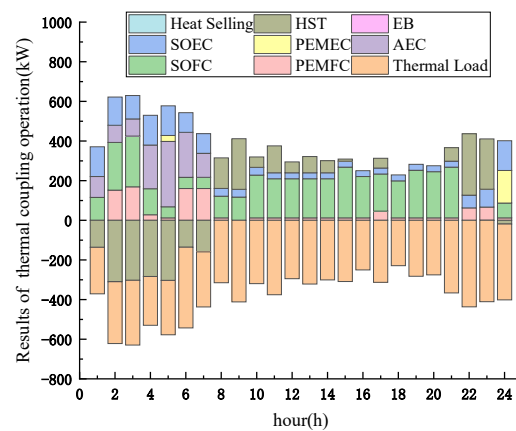


Figure 15. Thermal coupling operation results from fault scenarios without considering extreme scenario configuration.

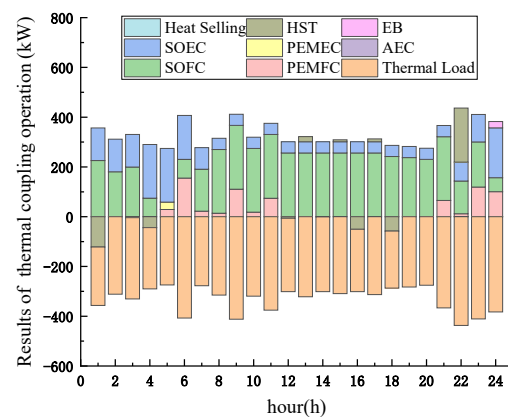


Figure 16. Thermal coupling operation results from fault scenarios considering extreme scenario configuration.

According to the hydrogen coupling operation results (Figures 19–22), in the fault scenario, the hydrogen energy storage output is greatly increased after considering the fault scenario configuration. The hydrogen storage capacity in the non-fault period of the photovoltaic equipment and the wind turbine and the hydrogen release amount in the fault period are increased to meet the needs of high-temperature solid oxide fuel cells. Compared with the normal scenario, the system does not sell hydrogen, and the hydrogen energy is mainly provided by the high-temperature solid oxide electrolytic cell

and the hydrogen storage tank, which mainly supply the high-temperature solid oxide fuel cell. In the normal scenario, the proton exchange membrane fuel cell, the proton exchange membrane electrolytic cell, and the alkaline electrolytic cell also participate in the conversion of hydrogen energy, and most of the hydrogen energy generated is sold. The decision concerning whether to consider the configuration of the fault scenario in the normal scenario has little effect on the running state of each device.

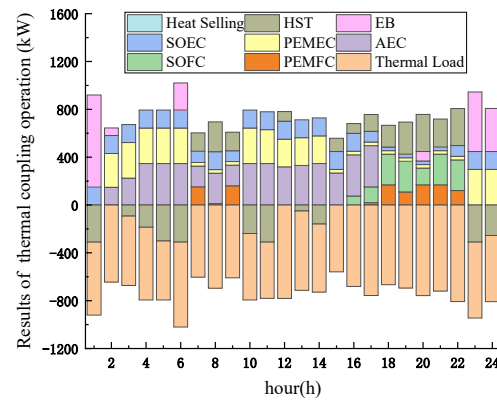


Figure 17. Thermal coupling operation results from normal scenarios without considering extreme scenario configuration.

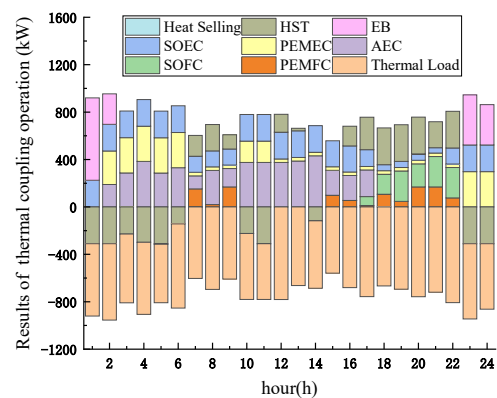


Figure 18. Thermal coupling operation results from normal scenarios considering extreme scenario configuration.

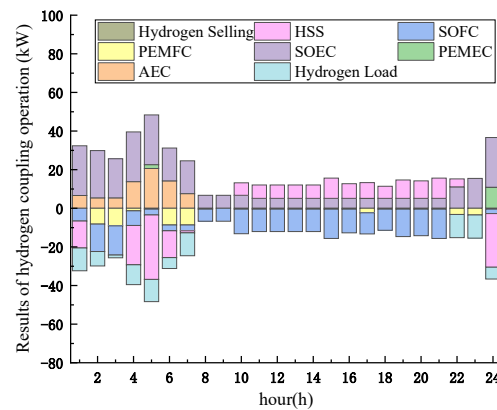


Figure 19. Hydrogen coupling operation results from fault scenarios without considering extreme scenario configuration.

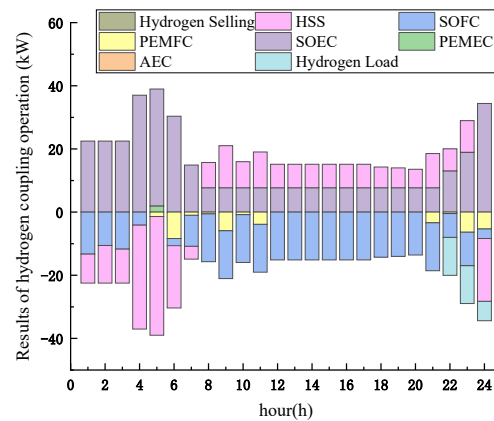


Figure 20. Hydrogen coupling operation results from fault scenarios considering extreme scenario configuration.

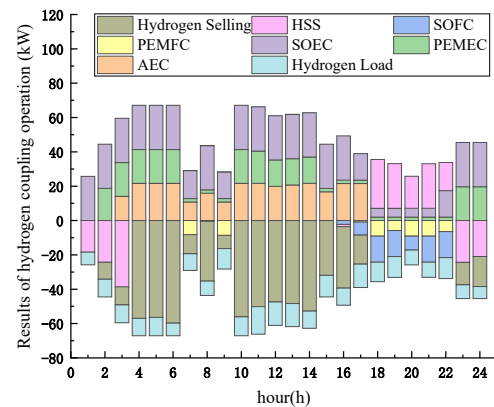


Figure 21. Hydrogen coupling operation results from normal scenarios without considering extreme scenario configuration.

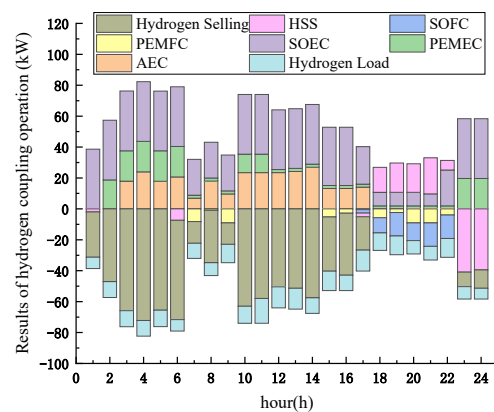


Figure 22. Hydrogen coupling operation results from normal scenarios considering extreme scenario configuration.

Energy Storage Operation Analysis

According to the above analysis, whether the fault scenario configuration is considered or not has a great influence on the capacity configuration results of energy storage equipment. Further analysis of the operating status of the electric energy storage, thermal energy storage, and hydrogen energy storage in the two cases in the fault scenario was conducted.

From Figures 23–25, it can be seen that after considering the configuration of the fault scenario, the charge and discharge of the electric energy storage increase, but the

re-discharge heat of the thermal energy storage decreases, and the full hydrogen of the hydrogen storage is not very different from that of the unconfigured fault scenario; after the fault scenario configuration, the power storage capacity of the electric energy storage increases at each moment, the heat storage capacity of the thermal energy storage decreases at each moment, and the hydrogen storage capacity of the hydrogen energy storage decreases at each moment, which further verifies the above analysis results regarding the electric, thermal, and hydrogen coupling operation.

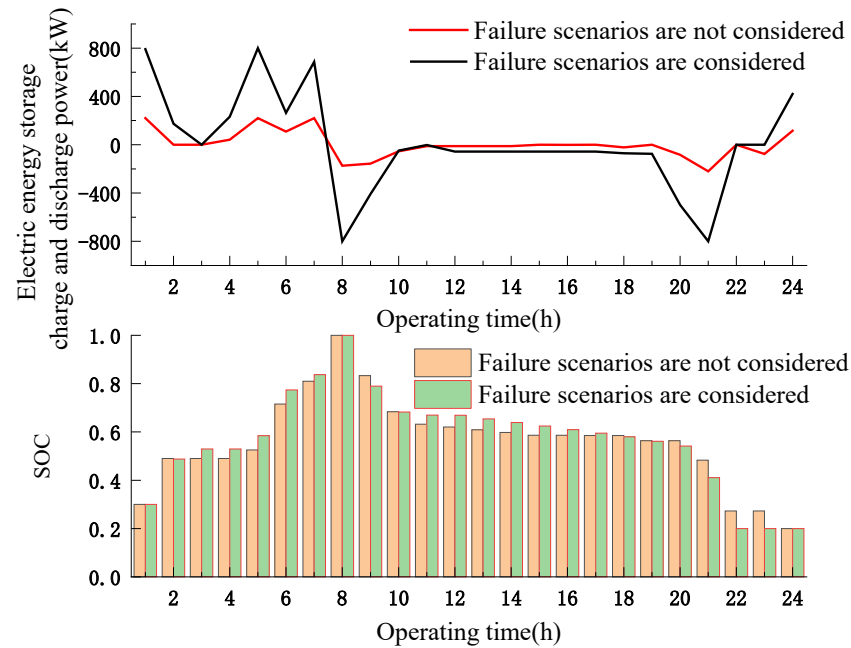


Figure 23. Working state of electric energy storage.

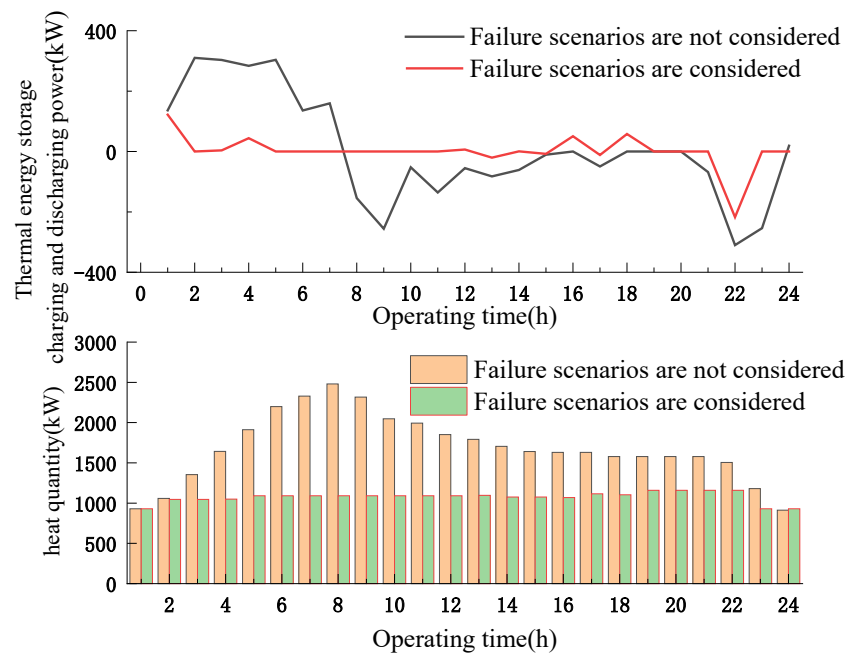


Figure 24. Working state of thermal energy storage.

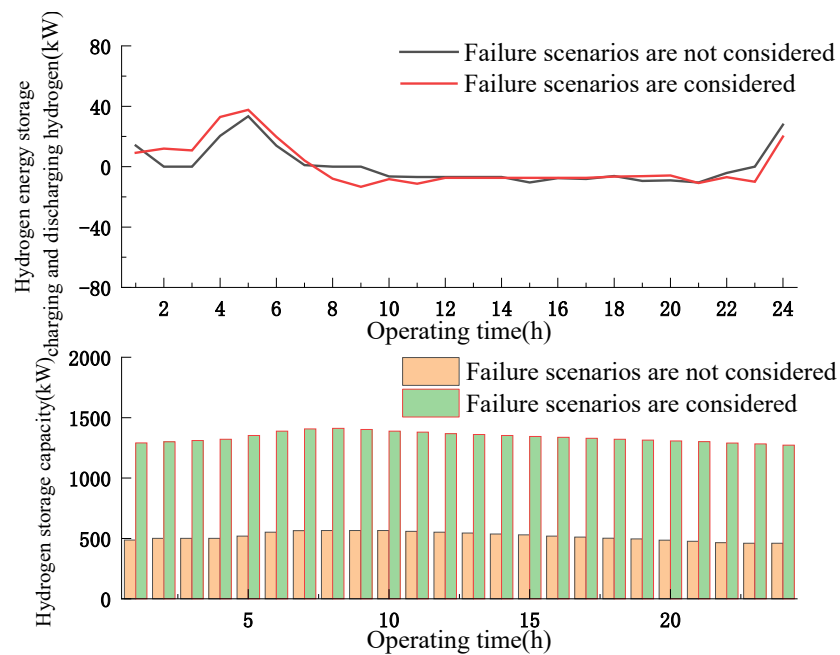


Figure 25. Working state of hydrogen energy storage.

6. Conclusions

In this study, which considered extreme fault scenarios, an optimal configuration method of energy storage for an electrothermal hydrogen integrated energy system was proposed, and the tabu chaotic quantum particle swarm optimization algorithm was used to solve the problem. Through the analysis of the examples, the following conclusions can be drawn:

When the tabu chaotic quantum particle swarm optimization algorithm is used to solve the two-layer capacity optimization problem, it has better global convergence and local convergence than the traditional particle swarm optimization algorithm and can ensure the reliability and accuracy of the results.

With the consideration of the extreme fault scenarios in the configuration layer, the configuration capacity of the various energy storage devices increases, and the energy storage output increases during the operation of the fault scenario, which further meets the load demand, reduces the load loss, and improves the resilience of the system while ensuring economy.

When the fault time of the wind power and photovoltaic power generation equipment is long, the reserve energy of the energy storage is not enough to supply the entire load demand during the fault period; the load loss of the system is large, and the system resilience needs to be further improved. At the same time, when focusing on reducing a certain type of load, the energy storage capacity configuration can be adjusted by changing the load loss penalty coefficient.

We recommend the design of energy storage systems with extreme disaster scenarios in mind to enhance resilience, optimize capacity through the adjustment of load loss penalties, and employ the tabu chaotic quantum particle swarm optimization algorithm for robust solutions. This study also underscores the necessity of including life degradation models in the system design. Future research should validate these findings through pilot projects, refine the optimization algorithms, and assess the impact of policies on resilient energy systems.

Author Contributions: Conceptualization, Z.C. and Z.S.; methodology, Z.C. and Z.S.; software, Z.S.; validation, D.L., Z.L. and J.C.; formal analysis, D.L.; investigation, Z.L.; resources, D.L.; data curation, Z.L. and J.C.; writing—original draft preparation, Z.S.; writing—review and editing, Z.C., D.L., Z.L. and J.C.; visualization, Z.C.; supervision, J.C.; project administration, D.L.; funding acquisition, Z.L. All authors have read and agreed to the published version of the manuscript.

Funding: This work was supported by research on coordinated optimal configuration and operation control technology for long-term and short-term hybrid energy storage considering multi-time scale matching requirements, Science and Technology Project of State Grid Zhejiang Electric Power Co., Ltd. (No. 5211DS230001).

Institutional Review Board Statement: Not applicable.

Informed Consent Statement: Not applicable.

Data Availability Statement: Data are contained within the article.

Conflicts of Interest: Authors Zhe Chen, Da Lin and Zhihao Li were employed by State Grid Zhejiang Electric Power Research Institute. The remaining authors declare that the research was conducted in the absence of any commercial or financial relationships that could be construed as a potential conflict of interest.

References

- Gu, W.; Wu, Z.; Bo, R.; Liu, W.; Zhou, G.; Chen, W.; Wu, Z. Modeling, planning and optimal energy management of combined cooling, heating and power microgrid: A review. *Int. J. Electr. Power Energy Syst.* **2013**, *54*, 26–37. [\[CrossRef\]](#)
- Yan, G.; Liu, D.; Li, J.; Mu, G. A cost accounting method of the Li-ion battery energy storage system for frequency regulation considering the effect of life degradation. *Prot. Control Mod. Power Syst.* **2018**, *3*, 43–51. [\[CrossRef\]](#)
- Nunna, H.S.V.S.K.; Doolla, S. Demand Response in Smart Distribution System with Multiple Microgrids. *IEEE Trans. Smart Grid* **2012**, *3*, 1641–1649. [\[CrossRef\]](#)
- Ni, L.; Liu, W.; Wen, F.; Xue, Y.; Dong, Z.; Zheng, Y.; Zhang, R. Optimal operation of electricity, natural gas and heat systems considering integrated demand responses and diversified storage devices. *J. Mod. Power Syst. Clean Energy* **2018**, *6*, 423–437. [\[CrossRef\]](#)
- Mohtaram, S.; Wu, W.; Aryanfar, Y.; Yang, Q.; Alcaraz, J.L.G. Introducing and assessment of a new wind and solar-based diversified energy production system intergrading single-effect absorption refrigeration, ORC, and SRC cycles. *Renew. Energy* **2022**, *199*, 179–191. [\[CrossRef\]](#)
- Wang, Y.; Qin, Y.; Ma, Z.; Wang, Y.; Li, Y. Operation optimisation of integrated energy systems based on cooperative game with hydrogen energy storage systems. *Int. J. Hydrogen Energy* **2023**, *48*, 37335–37354. [\[CrossRef\]](#)
- Wang, J.; Zeng, A.; Wan, Y. Multi-Time-Scale Optimal Scheduling of Integrated Energy System Considering Transmission Delay and Heat Storage of Heating Network. *Sustainability* **2023**, *15*, 14260. [\[CrossRef\]](#)
- Xiao, B.; Gao, Z.; Peng, H.; Chen, K.; Li, Y.; Liu, K. Robust Optimization of Large-Scale Wind–Solar Storage Renewable Energy Systems Considering Hybrid Storage Multi-Energy Synergy. *Sustainability* **2024**, *16*, 243. [\[CrossRef\]](#)
- Shi, Q.; Ding, J.; Liu, K.; Yan, W. Economic optimal operation of microgrid integrated energy system with electricity, gas and heat storage. *Electr. Power Autom. Equip.* **2019**, *39*, 269–276.
- Teng, Y.; Sun, P.; Luo, H.; Chen, Z. Autonomous optimization operation model for Multi-source microgrid considering electrothermal hybrid energy storage. *Proc. CSEE* **2019**, *39*, 5316–5324.
- Gu, W.; Wu, Z.; Yuan, X. Microgrid economic optimal operation of the combined heat and power system with renewable energy. In Proceedings of the IEEE PES General Meeting, Minneapolis, MN, USA, 25–29 July 2010; pp. 1–6.
- Zhou, Y.; Min, C.; Wang, K.; Xie, L.; Fan, Y. Optimization of integrated energy systems considering seasonal thermal energy storage. *J. Energy Storage* **2023**, *71*, 108094. [\[CrossRef\]](#)
- He, C.; Wu, L.; Liu, T.; Shahidehpour, M. Robust co-optimization scheduling of electricity and natural gas systems via ADMM. *IEEE Trans. Sustain. Energy* **2017**, *8*, 658–670. [\[CrossRef\]](#)
- Correa-Posada, C.M.; Sánchez-Martín, P. Integrated power and natural gas model for energy adequacy in short-term operation. *IEEE Trans. Power Syst.* **2015**, *30*, 3347–3355. [\[CrossRef\]](#)
- Algieri, A.; Beraldi, P.; Pagnotta, G.; Spadafora, I. The optimal design, synthesis and operation of polygeneration energy systems: Balancing life cycle environmental and economic priorities. *Energy Convers. Manag.* **2021**, *243*, 114354. [\[CrossRef\]](#)
- Zhou, J.; Wu, Y.; Zhong, Z.; Xu, C.; Ke, Y.; Gao, J. Modeling and configuration optimization of the natural gas-wind-photovoltaic-hydrogen integrated energy system: A novel deviation satisfaction strategy. *Energy Convers. Manag.* **2021**, *243*, 114340. [\[CrossRef\]](#)
- Liu, S.; Zhou, C.; Guo, H.; Shi, Q.; Song, T.E.; Schomer, I.; Liu, Y. Operational optimization of a building-level integrated energy system considering additional potential benefits of energy storage. *Prot. Control Mod. Power Syst.* **2021**, *6*, 1–10. [\[CrossRef\]](#)
- Li, Y.; Liu, C.; Zhang, L.; Sun, B. A partition optimization design method for a regional integrated energy system based on a clustering algorithm. *Energy* **2021**, *219*, 119562. [\[CrossRef\]](#)

19. Chen, H.; Chen, S.; Li, M.; Chen, J. Optimal Operation of Integrated Energy System Based on Exergy Analysis and Adaptive Genetic Algorithm. *IEEE Access* **2020**, *8*, 158752–158764. [[CrossRef](#)]
20. Ge, H.; Liu, F.; Chen, H.; Zhang, C. Coordinated optimization of district electricity and heating system based on genetic algorithm. In Proceedings of the IEEE PES Asia-Pacific Power and Energy Engineering Conference (APPEEC), Xi'an, China, 25–28 October 2016; pp. 1543–1547.
21. Fu, C.; Lin, J.; Song, Y.; Zhou, Y.; Mu, S. Model predictive control of an integrated energy microgrid combining power to heat and hydrogen. In Proceedings of the 2017 IEEE Conference on Energy Internet and Energy System Integration (EI2), Beijing, China, 26–28 November 2017; pp. 1–6.
22. Ubeda, J.R.; Allan, R.N. Sequential simulation applied to composite system reliability evaluation. *IEE Proc. Gener. Transm. Distrib.* **1992**, *139*, 81–86. [[CrossRef](#)]
23. Billinton, R.; Li, W. *Reliability Assessment of Electrical Power Systems Using Monte Carlo Methods*; Plenum: New York, NY, USA, 1994; pp. 60–66.
24. Rubinstein, R.Y. *Simulation and the Monte Carlo Methods*; Wiley: New York, NY, USA, 1981; pp. 119–126.
25. Xu, Y.; Huang, S.; Wang, Z.; Ren, Y.; Xie, Z.; Guo, J.; Zhu, Z. Optimization based on tabu search algorithm for optimal sizing of hybrid PV/energy storage system: Effects of tabu search parameters. *Sustain. Energy Technol. Assess.* **2022**, *53*, 102662. [[CrossRef](#)]
26. Bagheri, A.; Bagheri, M.; Lorestani, A. Optimal reconfiguration and DG integration in distribution networks considering switching actions costs using tabu search algorithm. *J. Ambient Intell. Humaniz. Comput.* **2021**, *12*, 7837–7856. [[CrossRef](#)]
27. Si, Y.; Wang, R.; Zhang, S.; Zhou, W.; Lin, A.; Zeng, G. Configuration optimization and energy management of hybrid energy system for marine using quantum computing. *Energy* **2022**, *253*, 124131. [[CrossRef](#)]
28. Feng, Z.; Niu, W.; Cheng, C. Multi-objective quantum-behaved particle swarm optimization for economic environmental hydrothermal energy system scheduling. *Energy* **2017**, *131*, 165–178. [[CrossRef](#)]

Disclaimer/Publisher's Note: The statements, opinions and data contained in all publications are solely those of the individual author(s) and contributor(s) and not of MDPI and/or the editor(s). MDPI and/or the editor(s) disclaim responsibility for any injury to people or property resulting from any ideas, methods, instructions or products referred to in the content.